Published in final edited form as:

FASEB J. 2023 October ; 37(10): e23194. doi:10.1096/fj.202300486R.

Differential regulation of MAP2 by phosphorylation events in proline-rich versus C-terminal domains

RA DeGiosio[1], **PG Needham**[2], **OA Andrews**[3], **H Tristan**[3], **MJ Grubisha**[1], **JL Brodsky**[2], **C Camacho**[4], **RA Sweet**[1,5]

[1]Department of Psychiatry, University of Pittsburgh, Pittsburgh, PA, USA

[2]Department of Biological Sciences, University of Pittsburgh, Pittsburgh, PA, USA

[3]Department of Neuroscience, University of Pittsburgh, Pittsburgh, PA, USA

[4]Department of Computational and Systems Biology, University of Pittsburgh, Pittsburgh, PA, USA

[5]Department of Neurology, University of Pittsburgh, Pittsburgh, PA, USA

Abstract

MAP2 is a critical cytoskeletal regulator in neurons. The phosphorylation of MAP2 (MAP2-P) is well known to regulate core functions of MAP2, including microtubule (MT)/actin binding and facilitation of tubulin polymerization. However, site-specific studies of MAP2-P function in regions outside of the MT-binding domain (MTBD) are lacking. We previously identified a set of MAP2 phosphopeptides which are differentially expressed and predominantly increased in the cortex of individuals with schizophrenia relative to non-psychiatric comparison subjects. The phosphopeptides originated not from the MTBD, but from the flanking proline-rich and C-terminal domains of MAP2. We sought to understand the contribution of MAP2-P at these sites on MAP2 function. To this end, we isolated a series of phosphomimetic MAP2C constructs and subjected them to cell-free tubulin polymerization, MT-binding, actin-binding, and actin polymerization assays. A subset of MAP2-P events significantly impaired these functions, with the two domains displaying different patterns of MAP2 regulation: proline-rich domain mutants T293E and T300E impaired MT assembly and actin-binding affinity but did not affect MT-binding, while C-terminal domain mutants S426E and S439D impaired all three functions. S443D also impaired MT assembly with minimal effects on MT- or actin-binding. Using heterologous cells, we also found that S426 but not T293E- had a lower capability for process formation than the wild-type protein. These findings demonstrate functional utility of MAP2-P in the proline-rich

For questions and correspondence please contact: Robert A. Sweet, M.D., Mail: Biomedical Science Tower, Rm W-1645, 3811 O'Hara Street, Pittsburgh, PA 15213-2593, Express Mail: Biomedical Science Tower, Rm W-1645, Lothrop and Terrace Streets, Pittsburgh, PA 15213-2593, Phone:412-624-0064, Fax: 412-624-9910, sweetra@upmc.edu, Web: http://www.sweetlab.pitt.edu/.

Author Contributions

R. DeGiosio and R. Sweet conceived the idea for this study. P. Needham and J. Brodsky assisted in the purification of mutant MAP2C proteins. R. DeGiosio generated the plasmid constructs. R. DeGiosio performed the research and acquired the data with assistance from O. Andrews and H. Tristan. R. DeGiosio analyzed the data. R. DeGiosio drafted the manuscript with assistance from R. Sweet. M. Grubisha, J. Brodsky, and C. Camacho revised the manuscript.

Conflict of Interest

The authors declare no conflicts of interest.

and C-terminal domains and point to distinct, domain-dependent regulations of MAP2 function, which can go on to affect cellular morphology.

Keywords

Microtubules; actin; microtubule-associated proteins; cytoskeleton; mutagenesis; neurobiology

Introduction

Microtubules (MTs) represent the stabilizing backbone of neurons, and their remodeling underlies major aspects of neuronal morphogenesis, including neurite initiation and elongation[1], branching[2], and pruning[3], as well as dendritic spine stabilization and growth[4]. They are also critical to the formation and function of neurites, providing structural support as well as transporting and organizing various cargoes, including organelles and signaling cascade components. Thus, in order to understand broader mechanisms of neuronal morphogenesis and function, it is imperative to understand the function and regulation of the microtubule-associated proteins (MAPs) which manipulate MT dynamics and organization. Foremost among such regulators is microtubule-associated protein 2 (MAP2), a neuron-specific MAP which localizes to the somatodendritic compartment. MAP2 is well-known for its MT-polymerizing property[5–7], reducing the frequency and length of depolymerizing "catastrophe" events to enable stable growth of the polymer[8]. It additionally serves to crosslink MTs and actin, facilitating coordinated shifts in cytoskeletal structure such as during neurite initiation and outgrowth[9, 10]. Indeed, heterologous overexpression of MAP2, particularly MAP2C, in various cell types consistently results in formation of neurite-like protrusions from the soma[11–13], emphasizing the sufficiency of MAP2 to initiate neurites.

MAP2 is heavily regulated by phosphorylation, which varies across development[14] and in response to synaptic activity[15]. It is thought that phosphorylation allows MAP2 to mediate developmental and activity-dependent changes in dendritic morphology by rearranging cytoskeletal elements. The roles of MAP2 phosphorylation (MAP2-P) have largely been characterized on a protein-wide scale using phosphate labeling and *in vitro* kinase/phosphatase treatment. However, phosphomimicry through amino acid substitution can better resolve effects of site-specific MAP2-P. For example, a triple phosphomimetic MAP2C construct (S319E/S350E/S382E; "MAP2C-EEE") lacks MT-binding, exhibits altered subcellular localization, and has a severly diminished ability to induce neurites in N2a cells[10, 16].

The phosphorylated sites in MAP2C-EEE reside in the MT-binding domain (MTBD) of MAP2, which contains 3-4 imperfect MT-binding repeats. However, evidence indicates that the proline-rich and C-terminal domains, which flank the MTBD, are also necessary for proper interaction with MTs and process formation in cells. For example, sequence analysis conducted by Ferralli & Matus (1994)[17] demonstrated that the MTBD alone is insufficient for complete MT-binding in living cells, and that stepwise addition of flanking sequence yields a corresponding gradual increase in MT-binding. Moreover, in the highly homologous MAP Tau, phosphomimicry within its proline-rich domain and C-terminal domains alters

MT-binding and tubulin polymerization[18, 19]. Despite these data, it is unknown how site-specific phosphorylation of MAP2 in domains flanking the MTBD regulates the function of this essential protein.

We recently identified a series of MAP2-P phosphopeptides from the proline-rich and C-terminal domains which are present in healthy individuals but are predominantly upregulated in individuals with schizophrenia[20]. Moreover, a subset of these phosphopeptides (containing a cumulative 10 putative phosphosites) negatively correlated with dendritic spine density and the socioeconomic status of subjects. These data suggest that these site-specific modifications represent normative regulatory mechanisms which are dysregulated in schizophrenia; however, the putative phosphosites have yet to be functionally characterized. We therefore sought to investigate the effects of identified MAP2-P sites on fundamental protein function. We isolated 10 MAP2C constructs which independently mimicked the putative MAP2-P events and subjected them to tubulin polymerization, MT-binding, actin-binding and actin polymerization assays. We additionally assessed a proline-rich and C-terminal domain mutant for process formation in HEK293T cells. We found that a subset of these constructs differentially impaired these activities, revealing domain- and site-specific patterns of MAP2 regulation by phosphorylation.

Materials & Methods

Preparation of Expression Constructs

IRES-MAP2C-EGFP plasmid containing cDNA encoding untagged human MAP2C (NM_031845) was purchased from GeneCopoeia™ (Cat#: CS-E2438-M61-01). For cell-free assays, the MAP2C coding sequence was PCR amplified using restriction site-containing primers (NdeI-MAP2C-XhoI, Table 1) and cloned into the bacterial expression vector pET21a (Novagen) at the NdeI and XhoI sites to generate pET21a_MAP2C. Phosphomimetic mutations were subsequently made using the QuikChange Lightening site-directed mutagenesis kit (Agilent) according to the manufacturer's instructions with mutagenic primers (Table 1). To perform the process formation assay, phosphomimietic mutations were made directly in the IRES-MAP2C-EGFP plasmid. Threonine residues were mutated to glutamic acid while serine residues were mutated to aspartic acid, with the exception of S426, which was mutated to glutamic acid in keeping with our prior studies of this site[20]. Plasmids were purified using the Qiagen Plasmid Maxi Kit (Qiagen). The presence of the mutations at the desired sites without additional off-target effects was confirmed by Sanger sequencing. Throughout this manuscript, all MAP2 residues are numbered according to the short MAP2C isoform (Uniprot P-11137-2) unless otherwise noted.

MAP2C Expression and Isolation

pET21a_MAP2C plasmids were transformed into BL21(DE3) bacteria (New England Biolabs). Overnight cultures were diluted 1:100 into Luria broth + ampicillin (100 μg/mL), then grown to OD600 ≈ 0.4-0.5. Isopropyl β-d-1-thiogalactopyranoside was added to a final concentration of 0.5 mM and the cultures were grown for a further 5 hr. MAP2C was subsequently purified as described[8] with minor modifications. In brief, cell pellets

were lysed in lysis buffer (50 mM Tris-HCl, pH = 8.0, 2 mM EDTA, 0.1% Triton) supplemented with 2 mg/mL lysozyme and 1X cOmplete mini protease inhibitor cocktail (Millipore Sigma) on ice for 20 min. Samples were sonicated and then centrifuged at 25,000g at 4°C for 10 min. NaCl and β-mercaptoethanol were added to the supernatant to final concentrations of 0.75 M and 2%, respectively. The supernatants were then heated at 95°C for 10 min, centrifuged at 10,000 rpm for 5 min in a microfuge at room temperature, and the buffer was exchanged into elution buffer (50 mM HEPES, pH = 7.4, 1 mM $MgCl_2$, 1 mM EGTA, 1 mM EDTA, and 2 mM β-mercaptoethanol) by way of a PD-10 column (GE Healthcare) per the manufacturer's instructions. MAP2 is an intrinsically disordered protein which lacks a native folded conformation; therefore, boiling in high salt denatures and eliminates the majority of bacterial proteins without risk of denaturing or unfolding MAP2. The MAP2 fractions were aliquoted and frozen at −80°C prior to assays. We verified that this procedure generated intact and highly enriched MAP2C by Coomassie-staining of SDS-polyacrylamide gels (see below) and western blot (performed as previously described[20]) (Figure 1). Protein concentration was determined by Pierce BCA Protein assay (Thermo Fisher Scientific) using bovine serum albumin as the standard. Prior to performing the indicated assays, the proteins were freshly thawed, diluted, and blinded to the experimenter (RAD).

Tubulin Polymerization Assay

In vitro tubulin polymerization assays were performed using the Tubulin Polymerization Assay Kit (Cytoskeleton Inc, cat# BK006P) according to the manufacturer's instructions with modification. A reaction containing 75 μL ice-cold tubulin (375 μg) diluted in general tubulin buffer (GTB; 80 mM PIPES, pH 6.9, 2 mM $MgCl_2$ and 0.5 mM EGTA) supplemented with 1 mM GTP was combined with 12.5 μL of MAP2C (5 μg) diluted in elution buffer in a half-area 96-well plate (Corning) for a total volume of 87.5 μL and for a final concentration of 86 μM tubulin and 1.2 μM MAP2. A higher final concentration of tubulin (5 mg/mL) than recommended was used to promote MT polymerization in the absence of glyercol and thus maximize efficient MAP2-tubulin interaction. The optical density at 340 nm (OD_{340}) was measured once per min for 1 hr at 37°C. MAP2C-lacking reactions were included as negative controls. All reactions were performed in technical duplicate (two wells per plate) in 4-5 independent assays.

For analysis, technical replicates were averaged and baseline-subtracted (yielding a single value for each biological replicate; N = 4-5 per genotype). OD_{max} was defined as the highest OD_{340} measurement. Tenth time ($t_{1/10}$) and the rate constant of elongation (k_{obs}) were derived as described in Bonfils et al (2007)[21], and $t_{1/10}$ is defined as the time at which one tenth of the final polymer has been generated, and here reflects the time at which $OD_{340} = (0.1 * OD_{max})$. k_{obs} is a pseudo first-order rate constant derived by assuming that the concentration of assembly-competent MT ends remains constant through the reaction, and equals the slope of the linear fit to $\ln(1-OD_t/OD_{max})$ against time. Datapoints in a 15-min window starting at $t_{1/10}$ were used for k_{obs} estimation.

Microtubule-Binding Assay

An *in vitro* MT-binding assay was performed using the Microtubule Binding Protein Spin Down Assay Kit (Cytoskeleton Inc, cat# BK029) according to the manufacturer's instructions. MTs were freshly polymerized from 100 μg monomeric tubulin diluted in a total volume of 224 μL GTB supplemented with 20 μM taxol and 0.5% glycerol and kept at room temperature prior to use. For each reaction, 20 μL of freshly prepared MTs (which contain 11 μg tubulin dimers) were incubated with 12.5 μL of MAP2C (5 ug) diluted in elution buffer for 30 min at room temperature in GTB supplemented with 1 mM GTP, for a total volume of 50 μL so that the final concentrations in the assay were 2.2 μM tubulin dimers and 2 μM MAP2. MAP2C-only reactions were included as negative controls (data not shown). Reaction solution was then placed on top of a 100 μL taxol-supplemented cushion buffer (80 mM PIPES, pH 7.0, 1 mM $MgCl_2$, 1 mM EGTA, 60% glycerol) and centrifuged at 100,000g for 40 min at room temperature. The supernatants were removed, and MT-containing pellets were resuspended in 1x SDS sample buffer for analysis.

Samples were run on TruPAGE 4-20% precast SDS-PAGE gels (Sigma) and stained using SimplyBlue SafeStain (Invitrogen). Stained gels were photographed on a lightbox with a Canon PowerShot G5X camera. The images were converted to greyscale and densitometric analysis was performed using ImageJ software (NIH, RRID: SCR_003070). Pull-down efficiency was defined as the optical density of MAP2 in the pellet (P) fraction divided by the optical density of tubulin in the same fraction (Tub). The relative level of pull-down was normalized to the level of wild type (WT) MAP2 material pulled-down within the same gel. Mutants of the "red" group (S426, S429, S443, S446) were run across two gels with a WT control condition in each, leading to an N = 6 for WT within this group (Figure 3G).

Actin-Binding Assay

In vitro actin-binding assays were performed using the Actin-binding Protein Spin Down Assay Kit using human platelet actin (Cytoskeleton Inc, cat# BK013) according to the manufacturer's instructions. Actin was freshly polymerized (generating filamentous [F-] actin) from 250 μg G-actin diluted in 250 μL general actin buffer (GAB; 5 mM Tris-HCl pH 8.0, 0.2 mM CaCl) supplemented with 0.2 μM ATP and 1X actin polymerization buffer (ABP; final concentrations of 50 mM KCl, 2 mM $MgCl_2$, 5 mM guanidine carbonate, pH 7.5, 1 mM ATP, and 10 mM Tris, pH 7.5) and kept at room temperature prior to use. For each reaction, 40 μL F-actin stock (prepared from 40 μg G-actin) was incubated with 10 μL MAP2C (4 μg) diluted in elution buffer for 30 min at room temperature for a total volume of 50 μL, which contained the equivalent of 19 μM G-actin and 1.6 μM MAP2. MAP2C-only reactions were included as negative controls (data not shown). Reactions were then centrifuged at 100,000g for 40 min at room temperature. The supernatants were separated and the F-actin-containing pellet fractions were resuspended in 1x SDS sample buffer for analysis. Samples were subsequently analyzed as for the *Microtubule Binding Assay*, with pull-down defined as the density of MAP2 divided by the density of actin in the pellet fraction (P/F-actin). As for the *Microtubule-Binding* Assay, mutants of the "red" group (S426, S429, S443, S446) were run across two gels with a WT control condition in each, leading to an N = 10 for WT within this group (Figure 4G).

Actin Polymerization Assay

In vitro actin polymerization assays were performed using the Actin Polymerization Kit (Cytoskeleton Inc, cat# BK003) according to the manufacturer's instructions with modification. Pyrene G-actin was thawed, diluted in GAB supplemented with 20 μM ATP, left on ice for 1 hr, then ultra-centrifuged at 100,000g, 4°C for 1 hr to eliminate all polymerized actin prior to beginning the assay. A total of 200 μL pyrene G-actin (44 μg) was combined with 20 μL MAP2C (amounts specified in figures) diluted in elution buffer in a black 96-well assay plate (Corning) for a total volume of 220 μL such that the final concentrations of G-actin and MAP2 were 4.7 μM and 0.05-0.4 μM respectively. For control reactions, 20 μL GAB was substituted for MAP2. As a positive control, 1 μM jasplakinolide (Cayman) in 20 μL elution buffer was added in place of MAP2. Kinetic fluorescence readings at 350 nm excitation, 405 nm emission were made once per min for 5 min on a fluorometer (Biotek). Actin polymerization buffer was then added to 0.5X (final concentrations [mM]: 21 KCl, 0.8 $MgCl_2$, 2 guanidine carbonate, 0.4 ATP) and readings continued once per minute for 1 hr. Reactions lacking actin polymerization buffer or MAP2C were included as negative controls. All reactions were performed in technical duplicate (two wells per plate) in 3-5 independent biological replicate assays, yielding N = 6-10 per genotype.

For analysis, two output measures were calculated as described in Doolittle et al (2013)[22]: the half-time ($t_{1/2}$) and the rate of actin polymerization at $t_{1/2}$ ($AP_{1/2}$). Similarly to $t_{1/10}$, $t_{1/2}$ is defined as the time at which one half of the final actin polymer has been generated. In brief, to derive $t_{1/2}$, minimum intensity (I_{min}) was estimated by averaging intensity readings obtained during the 5-min baseline measurement period, and maximum intensity (I_{max}) was estimated by averaging the times at which the ten highest readings were observed, then averaging the ten intensity readings closest to this mean time. A line was then fit to datapoints between $(0.4 * (I_{max} - I_{min}) + I_{min})$ and $(0.6 * (I_{max} - I_{min}) + I_{min})$. $t_{1/2}$ was calculated using the resulting slope ($m_{1/2}$) and intercept ($b_{1/2}$) as: $(0.5 * (I_{max} - I_{min}) + I_{min} + b_{1/2})/m_{1/2}$. Next, to calculate $AP_{1/2}$, a scaling factor (SF) between fluorescence intensity and units of filament concentration was calculated as $(4.58/(I_{max} - I_{min}))$, where 4.58 represents the differential between the starting concentration of actin in the assay and the critical concentration (assuming a k_+ and k_- of 11.6 μM^{-1} s^{-1} and 1.4 s^{-1} [23]). $AP_{1/2}$ was subsequently calculated as $(SF * m_{1/2})$.

Cell Culture & Transfection

HEK293T cells (RRID: CVCL_0063) were purchased from ATCC (cat# CRL_3216, RRID: CVCL_0063), maintained in complete media (RPMI-1640 [Gibco] + 5% fetal bovine serum [Thermo Fisher]) at 37°C, with 5% CO_2, and passaged every 2-4 days to maintain subconfluent culture. For transfection, cells were plated at 10^5 cells per well in 12-well plates containing poly-D-lysine (PDL)-laminin coated glass coverslips and incubated in complete media. The next day, plasmid DNA (1 μg per well) and Lipofectamine 2000 Reagent (Invitrogen; cat#:11668027; 2 μL per well) were combined in 100 uL OPTI-MEM media (Gibco) per well and left to incubate at room temperature for 25 min to create a transfection mixture. Transfection mixtures were added to the wells dropwise and plates

were returned to the incubator for 2 hours before the well contents were replaced with fresh complete media.

Immunocytochemistry

Cells were harvested 48 hours after transfection. After a quick wash in PBS, coverslips were fixed in 4% paraformaldehyde (supplemented with 0.1% Triton, to extract excess unpolymerized tubulin protein) for 20 minutes, washed 3 times for 5 minutes in PBS, then permeabilized with 0.2% Triton for 10 minutes and again rinsed 3 times for 5 minutes in PBS. Coverslips were blocked for 1 hour in PBS containing 2% normal goat serum (Jackson ImmunoResearch Laboratories, Inc.), then changed into primary antibody solution (PBS with 1% normal goat serum, 1:2000 rabbit anti-β-tubulin [Abcam, cat# ab6046], and 1:500 mouse anti-MAP2 [Abcam cat# ab11267]) and incubated at 4°C overnight. After another three washes with PBS, coverslips were incubated for 90 minutes at room temperature in secondary antibody solution (PBS with 1% normal goat serum, 1:1000 goat anti-mouse Alexa Fluor 568 [Invitrogen; cat# A11031], and 1:1000 goat anti-mouse Alexa Fluor 405 [Invitrogen; cat# A-31553]). After a final three rinses in PBS, the coverslips were mounted onto glass slides with Vectashield HardSet Antifade Mounting Medium (Vector Laboratories; cat# H1400). Slides were blinded prior to imaging.

Confocal Imaging & Image Processing

Data acquisition was performed using Slidebook 6.0 software (Intelligent Imaging, RRID:SCR_014423) on an Olympus (Center Valley, PA) BX51 WI upright microscope equipped with an Olympus spinning disk confocal (SDCM) using an Olympus PlanAPO N 10X 0.40 NA air objective and a 1.42 numerical aperture 60X oil supercorrected objective. 60X image stacks with a step size of 0.25 μm were taken through the entirety of each cell. At each plane, data were collected in the 405 nm (MAP2), 488 nm (GFP) and 568 nm (tubulin) channels. Exposure times for the 488 nm channel was optimized for each cell based on best spread of histogram intensity data. Exposure time for the 405 nm and 568 nm channels was optimized with a WT MAP2C-transfected cell and was maintained for all subsequent cells (MAP2: 130 ms, neutral density = 2; β-tubulin: 100 ms, neutral density = 2).

405 nm (MAP2) and 568 nm (β-tubulin) signals were deconvolved using the Autoquant blind deconvolution algorithm in Slidebook. The Z-plane with best GFP focus was then cropped for further processing. Ridler-Calvard values were used to generate masks of all channel signals. These signals were added together and inverted to generate a background mask. Any other GFP-positive cells in the field of view were removed from the 488 nm channel mask (GFP) to generate the ROI mask from which MAP2/β-tubulin mean intensity data was extracted. Neurite-like processes were manually counted. Such processes were defined as MT+ cellular protrusions >10 μm in length and <4 μm in maximum width. For all analyses, N = 57-59 cells were examined per genotype across three independent experiments.

Statistical Analysis

Ratios of MAP2C to tubulin/actin (P/Tub, P/F-actin) as well as tubulin polymerization metrics $t_{1/10}$, and k_{obs} were compared between the WT protein and other conditions by one-way ANOVAs with Dunnett's post-hoc tests performed using Graphpad Prism software (RRID:SCR_002798). To assess relative MT- and actin-binding affinities, P/Tub and P/F-actin values were compared within each genotype by independent Student's t-tests. For actin polymerization data, $t_{1/2}$ and $AP_{1/2}$ were compared between the control reaction lacking MAP2 and other conditions by two-way ANOVAs testing for main effects of condition and pipetting order (we observed significant correlations between pipetting order and $t_{1/2}$ (r_{128} = .339, $p < 0.001$) or $AP_{1/2}$ (r_{128} = −.405, $p < 0.001$), likely due to time-dependent hydrolysis of ATP in the reaction buffer) with Dunnett's post-hoc tests in IBM SPSS (IBM, RRID:SCR_002865). For comparison of MAP2/β-tubulin intensities, one-way ANOVAs with condition and round as fixed effects were performed in IBM SPSS. To test for differences in process formation, a Chi-square test was performed in GraphPad Prism. All statistical tests were two-sided with $\alpha = 0.05$. Data are displayed as mean ± standard error of mean (SEM) unless otherwise noted.

Results

MAP2-P in MTBD-flanking regions slows MT assembly kinetics.

We first used our bacterially-expressed, highly enriched WT MAP2C and the phosphomimetic MAP2C constructs to ascertain effects of MAP2-P in the proline-rich and C-terminal domains (Figure 2A) on one of the foremost functions of MAP2: the facilitation of MT assembly. The optical density of a solution of tubulin monomers is tracked across time as a proxy for MT polymerization/bundling (Figure 2B–D). We saw that the presence of WT MAP2C reduces the tenth time ($t_{1/10}$; time to generate one tenth of final polymer product) by up to 72% relative to a MAP2-lacking control reaction (Figure 2E–G). However, it does not alter the apparent pseudo-first order rate constant of MT elongation (k_{obs}; see Materials & Methods) (Figure 2H–J).

We found that phosphomimicry at several residues in the proline-rich (T293, T300) or C-terminal (S426, S439 and S443) domain was capable of altering both $t_{1/10}$ and k_{obs}. T293, S426 and S443 increased $t_{1/10}$ and decreased k_{obs}. T300 and S439 increased $t_{1/10}$ without altering k_{obs} (Figure 2E–J). This experiment thus identified a subset of MAP2-P events in the proline-rich and C-terminal domains—flanking the MTBD—which alter MAP2 function by impairing the facilitation of MT assembly.

MAP2-P in the C-terminal domain impairs MT-binding.

In vitro phosphorylation of MAP2 has long been known to impair tubulin polymerization and MAP2/MT-binding in tandem[24–26]. However, these studies have either examined MAP2-P on a protein-wide level or focused on sites within the MTBD. We hypothesized that the observed deficits in MT assembly resulting from MAP2-P in flanking domains would be associated with impaired MT binding. To test this hypothesis, we subjected our MAP2C constructs to an ultracentrifugation-based pull-down assay. WT MAP2C demonstrated robust pull-down with MTs under saturating conditions (molar ratio ~1:1

MAP2C/tubulin), with an average of 77% of the protein being found in the MT-containing pellet fraction across experiments (Figure 3A). We determined that three tested mutants within the C-terminal domain--S426E, S443D, and S446D—significantly impaired MT association, showing 14-32% reductions in pull-down efficiency (Figure 3G). In contrast, no significant changes in MT-binding were observed for any mutants of the proline-rich domain (Figure 3E), including those sites which slowed MT assembly kinetics (Figure 2C,F,I). These combined results indicate that MAP2-P can affect MT assembly through multiple avenues, either by simply promoting dissociation of the protein from tubulin, or by altering its function when docked onto MTs.

MAP2-P in MTBD-flanking regions impairs actin-binding.

It was previously indicated that MAP2-P in the MTBD which reduces the protein's association with MTs can conversely promote localization to actin networks[16]. However, such a function has not yet been investigated for MAP2-P events of the MTBD-flanking proline-rich and C-terminal domains. Therefore, we also measured the association of phosphomimetic MAP2C mutants with actin filaments by pull-down assay, hypothesizing that mutants with reduced MT-binding activity would exhibit a corresponding increase in actin-binding. As shown in Figure 4A, we observed an average efficiency of 36% in pull-down assays with WT MAP2. Contrary to our hypothesis, we found that phosphomimicry at two sites in the C-terminal region (S426 and S439) reduced the assocuation of MAP2C with actin (Figure 4F–G). Two proline-rich domain residues additionally reduced actin-binding: T293 and T300 (Figure 4D–E). For these residues, actin-binding activity was reduced by ~43%, whereas residues in the C-terminal domain exhibited a 10-24% reduction in actin. In combination with our data presented above, this demonstrates that individually phosphorylated MAP2 sites can reduce the protein's associations with MTs and actin filaments either independently or in tandem. To test this explicitly, we used Student's t-tests to compare the MT- and actin-binding ability of each construct. We confirmed that T293E and T300E alone showed significant differences between MT- and actin-binding (normalized to WT), indicating that they can downregulate actin-binding selectively (Figure 5).

WT MAP2 and MAP2-P do not affect actin polymerization.

We hypothesized that MAP2 plays a role in actin polymerization, and that MAP2 phosphorylated sites which impair actin-binding could also influence this process. We therefore tested WT and phosphomimetic MAP2C mutants in a fluorometric actin polymerization assay. Here, pyrene-labeled G-actin was used, the fluorescence of which increases 7-10 fold upon integration into filaments [27]. We observed no change in either $t_{1/2}$ (i.e., the time to generate half of total polymer) or $AP_{1/2}$ (i.e., the rate of polymerization) between a MAP2-negative control reaction and a reaction containing WT MAP2C at varying concentrations. In contrast, a positive control reaction using the actin-stabilizing agent jasplakinolide[28] exhibited a significant decrease in $t_{1/2}$ and an increase in $AP_{1/2}$ (Figure 6A–C). This result indicates that MAP2C is incapable of intrinsically promoting actin polymerization. Moreover, none of the phosphomimetic mutants differed from reactions lacking MAP (Figure 6D–F).

S426E MAP2 has reduced process formation ability relative to WT

Finally, given the importance of MT assembly and MT/F-actin crosslinking in neurite formation and outgrowth, we sought to determine whether the changes we observed in cell-free systems bore consequences for cellular morphology. The ability of MAP2C to form neurite-like processes in heterologous cell lines is well-established. Thus, we transfected HEK293T cells with WT, T293E or S426E MAP2C to examine their propensity towards process formation (Figure 7A). T293E and S426E were chosen to represent phosphorylation in the MTBD-proximal proline-rich domain and C-terminal domain, respectively, as these domains exhibited differential MT-binding ability (Figure 3).

First, we verified that proteins representing the three genotypes were expressed at comparable levels in these cells (Figure 7B). We also observed that tubulin levels did not vary by genotype (Figure 7C). As previously described for other heterologous cell lines, MAP2C-transfected cells showed tightly bundled MTs and frequently exhibited neurite-like, MT+ protrusions from the cell body (Figure 7D). A Chi-square test showed that the genotype significantly affected the proportion of cells with processes, with S426E MAP2C transfectants—but not T293E transfectants—more frequently lacking processes than WT transfects (Figure 7E).

Discussion

Here, we systematically investigated the *in vitro* function of a variety of MAP2C constructs which mimic MAP2-P events in the proline-rich and C-terminal domains. We isolated these constructs from bacteria before assessing their MT/actin assembling and binding activities in order to develop a fuller understanding of how MAP2-P in these regions influences the protein's association with cytoskeletal networks. Further, we tested two representative mutants for their process formation ability in heterologous cells to gauge whether these mutations have cellular consequences.

We identified a subset of phosphomimetic constructs which displayed reduced MT and/or actin-binding as well as slowed MT assembly kinetics, indicated by increased $t_{1/10}$ and decreased k_{obs}. Specifically, the MAP2-P sites we studied suggest two distinct functional outcomes depending on the targeted domain (Figure 8): 1) a reduction in MT assembly and loss of actin-binding despite sustained MAP2/MT-binding (resulting from proline-rich domain phosphorylation), or 2) partial dissociation of MAP2 from both MTs and actin (resulting from C-terminal domain phosphorylation). Additionally, C-terminal domain phosphorylation, specifically at S426E, was associated with reduced MAP2C-mediated process formation in HEK293T cells. Below we expand upon each of these modes of MAP2 regulation, and also discuss the mutants which lacked an observed effect.

Proline-Rich Domain Phosphorylation Sites Destabilize MTs without Impairing MAP2/MT-binding

Phosphomimicry at residues in the proline-rich domain, including T293 and T300, exhibited no change in MT-binding despite yielding significant impairment in MT assembly kinetics (Figures 2C,F,I & 3D,E). While novel to MAP2, a similar mechanism has been alluded

to in MAP Tau. Specifically, *in vitro* phosphorylation by Cdk2/CycA3, targeting AT8 and AT180 epitopes—the latter of which recognizes pT231 (homologous to MAP2 pT293)—has been shown to selectively impair MT assembly despite retaining MT-binding[29]. A role of Tau T231 has further been suggested by NMR spectroscopy[30, 31]. This structural data has indicated that pT231 induces a conformational change in the proline-rich domain via salt bridge formation with R230, which alters the interaction of the proline-rich domain with MTs. We previously observed an analogous salt bridge in a simulated model of pT293 MAP2 formed with the homologous R292 residue[20]. Moreover, pT231 in Tau promotes association with the prolyl isomerase, Pin1, which isomerizes the proline bond between *cis* and *trans* conformations, significantly altering the overall conformation of the protein[32, 33]. This could provide another possible mechanistic explanation for altered function. MAP2 T293, which is also followed by a proline (P294), may isomerize in a similar manner. Though an association between Pin1 and MAP2 has not, to our knowledge, been directly observed, we recently identified peptidylprolyl isomerase A (PPIA) as a MAP2 interactor in an unbiased proteomic screen of the MAP2 interactome[20].

Thus, phosphorylation at T293 or T300 allows dissociation of the MT-binding and assembling functions of MAP2. A functional role for such discrimination has not been proposed for Tau, but in the case of MAP2, it may be relevant in contexts which simultaneously require an attenuation of MT polymerization and/or bundling but also the maintained anchorage of proteins to the MT network. For instance, in long-term depression (LTD) induction, MAP2 is required for relocalization of the MT plus-end binding protein, EB3, to dendritic shafts. MT polymerization is attenuated during LTD, though the MAP2/MT association appears to be unimpaired[34]. Another such instance could include neurite branching. Formation of nascent neurite branches is accompanied by transient MT destabilization and remodeling, which is mediated by a variety of proteins that become enriched at branchpoints such as MT severing enzymes, septins, motor proteins, and plus end-binding proteins[2]. MAP2 may play a role in organizing/regulating such proteins while simultaneously downregulating its own MT-polymerizing function.

The effect of flanking domain residues on actin-binding is somewhat surprising, given that past work of Roger et al (2004)[35] indicated that the MTBD (a.a. 300-400) of MAP2 is sufficient for full actin-binding ability. Indeed, it is thought that the same domain coordinates both cytoskeletal networks; Tau appears to simultaneously bind MTs and F-actin at sequential, imperfectly repeating motifs within the MTBD[36]. However, MAP2-P events proximal to- but not within- the MTBD could sterically obstruct the interaction between this domain and actin, as opposed to altering actin-binding sites directly. Given that MT- and actin-binding sequences in Tau/MAP2 appear to strongly overlap, the unique ability of T293E and T300E to selectively downregulate actin-binding of MAP2 while preserving MT-binding (Figure 5) is notable. This suggests that, at least under our experimental conditions, MAP2 can use different binding modes to bind either MTs or F-actin within the same sequences. For instance, stoichiometries of the interactions may differ; C-terminal sites S426 and S439 reduce MT-binding affinity of MAP2C by nearly a third (Figure 3G), possibility reflecting a deactivation of one of the three imperfect repeat motifs of the MTBD present in MAP2C, while the proline-rich sites T293 and T300 reduce actin-binding affinity by

approximately half (Figure 4E), perhaps reflecting an ablation of one of two actin-binding sites.

Notably, the actin-binding activity of MAP2C does not promote actin filament formation, as actin filament assembly is unaffected in the presence of MAP2C (Figure 6). However, the actin-binding function of MAP2 is likely relevant for other reasons, such as its control of the subcellular localization of the protein (such as in actin-rich compartments like dendritic spines, which MAP2 is known to invade[37]), and the crosslinkage of MT and actin networks[38]. Thus, diminished actin-binding capacity following MAP2-P could belie a significant regulatory mechanism of use to neurons.

Strikingly, despite its observed impairments to MT assembly (Figure 2C,F,I) and actin-binding (Figure 4E), mutation at T293 does not appear to substantially affect process formation in heterologous cells (Figure 7E–F). This suggests that the role MAP2 plays in neurite initiation may not be limited to promoting MT growth and bundling, or even crosslinking MTs and F-actin. Instead, MAP2 may serve to anchor or modulate other proteins necessary for protrusion. One such protein could be protein kinase A (PKA), which promotes neuritogenesis when activated in neural progenitor, neuroblastoma or heterologous PC12 cells[39–41]. The presence of MAP2 on MTs may also enhance their flexural rigidity, which is thought to potentially facilitate the translocation of bundles into nascent processes by the motor protein dynein[42].

C-terminal Domain Phosphorylation Sites Weaken MAP2 Associations with Cytoskeletal Networks

Phosphomimicry at residues in the C-terminal domain, including S426 and S439, decreased MT and actin binding. This is generally consistent with Tau; S426 is homologous to Tau S396, a residue which when phosphorylated reduces the MT-binding affinity of the protein and moreover is implicated in synaptic plasticity[43, 44]. These sites fit within the traditional view of MAP2-P; namely, that it induces dissociation of the MAP from MTs to increase MT dynamics. This can modulate MT cytoskeleton stability during development and in response to certain extracellular signals. In contrast to the sites we studied in the proline-rich domain, such C-terminal MAP2-P events might additionally be expected to increase availability of the protein to associate with alternative binding partners, associations which are usually tightly controlled via the sequestration of MAP2 by MTs. For instance, we previously observed an association of MAP2 with ribosomal proteins by co-immunoprecipitation, which may have a functional role as MAP2C overexpression in HEK cells suppresses protein synthesis[20]. It is tempting to speculate that MAP2-P further enhances this interaction to regulate protein synthesis; indeed, we found indirect evidence of such an effect as mice bearing the S426E mutation in *MAP2* gene (a residue present in all MAP2 isoforms) have reduced levels of various synaptic proteins[20].

S426E bore the additional effect of reducing process formation aptitude of MAP2C in HEK293T cells (Figure 7E–F). As discussed above, this may be due to an impaired ability to anchor critical mediators to nascent projections, or reduced rigidity of formed MT bundles, both of which are subsequent to impaired MT-binding. Notably, these findings are consistent with our prior work on this mutant; CRISPR mice harboring the S426E mutation (S1782E

in the mature, high molecular weight isoform MAP2B) exhibit reduced dendritic length and complexity in the primary auditory cortex[20] . Our results suggest that such an effect originates early in development, at the stage of neurite initiation, when low molecular weight isoforms of MAP2 such as MAP2C are predominant[14]. This mirrors the presumed pattern of neuromorphological deficits in schizophrenia, where they are thought to accrue over development and predispose individuals to later environmental insults, as opposed to representing a degenerative process.

S443D also significantly impaired MT assembly (Figure 2D,G,J), yet had only a modest effect on MT- or actin-binding (~10-14% reductions; Figure 3G, Figure 4G). This further supports the idea that MAP2-P-induced suppression of MT assembly is not solely caused by dissociation of MAP2 protein from MTs, but can instead rely on a more subtle change in MAP2/MT interactions, as is suggested in the case of MAP2 pT293/Tau pT231 (see above). However, S443D did not share the ability of T293E/T300E to selectively downregulate actin-binding (Figure 5); thus, their respective effects on MT assembly likely result from distinct changes in MAP2 conformation.

Other Phosphorylated Sites Have No Effect On MAP2 Association With MTs Or Actin

Five of the ten sites investigated, T249, S252, Y253, S297, and S446, failed to affect any tested function of MAP2. T249, S252 and Y253 belong to the same peptide identified in our phosphoproteomic study, which is located in the proline-rich domain. This peptide is farther from the MTBD than the other sites from this domain, perhaps explaining the lack of an effect. These three sites are also not conserved in Tau, further supporting the idea that they are not essential for the interactions of MAP2 with MTs and actin, core functions which are shared with Tau. The association of this phosphopeptide with schizophrenia, however—concurrent with reduced spine density in primary auditory cortex—may indicate an alternate functional role for phosphorylation at these sites. This may include, for instance, regulation of MAP2 interactions with SH3 domain-containing proteins like EB3[34], which bind to proline-rich domains. Alternately, these sites may be incidental targets of upstream kinases and phosphatases which co-regulate the other, more efficacious phosphorylation sites. S297 and S446 may similarly be associated with nearby sites while not affecting MAP2 function directly. For instance, in Tau, S235 (homologous to MAP2 S297) is a known priming phosphorylation site, increasing subsequent phosphorylation at T231 (homologous to MAP2 T293) by GSK3β[45].

Conclusion

In conclusion, we identified a subset of unstudied MAP2-P events that impair the protein's association with both MTs and actin as well as its ability to promote the assembly of MTs. We describe two distinct, domain-dependent modes of MAP2 regulation, including attenuation of the MT-assembling function of MAP2 with retained MT-binding, or partial dissociation of MAP2 from both MTs and actin (Figure 8). Mutation of S426, but not T293, reduced MAP2C-mediated process formation in HEK293T cells, suggesting influences of MAP2 on neurite initiation independent of MT assembly or MT/F-actin crosslinking. These data provide novel insight into the regulation of MAP2 by phosphorylation at novel

sites and in understudied domains, as well as clues about how MAP2 protein associates with cytoskeletal filaments and subsequent consequences for cells. It remains to be seen how phosphomimetic MAP2 mutations go on to affect protein function in neurons both at baseline and in the context of synaptic activity. The analysis of upstream kinases/phosphatases responsible for MAP2-P at the sites studied will also represent an intriguing line of investigation going forward. Such studies could reveal targetable interactions or processes for novel therapeutic development to prevent or reverse cytoskeletal dysregulation in schizophrenia.

Acknowledgements

This work was supported by the National Institute of Mental Health (grant numbers: MH116046 and MH071533), the National Institute on Aging (grant number: AG027224), the National Institute of General Medical Sciences (grant number: GM131732) and the National Institute of Diabetes and Digestive and Kidney Diseases (grant number: DK079307). The content is solely the responsibility of the authors and does not necessarily represent the official views of the National Institutes of Health.

Data availability

The data that support the findings of this study are available from the corresponding author upon request.

References

1. Flynn KC The cytoskeleton and neurite initiation. Bioarchitecture 2013; 3:86–109. [PubMed: 24002528]
2. Kalil K, and Dent EW Branch management: mechanisms of axon branching in the developing vertebrate CNS. Nature Reviews Neuroscience 2014; 15:7–18. [PubMed: 24356070]
3. Rumpf S, Wolterhoff N, and Herzmann S Functions of microtubule disassembly during neurite pruning. Trends Cell Biol. 2019; 29:291–297. [PubMed: 30683460]
4. Dent EW Dynamic microtubules at the synapse. Curr. Opin. Neurobiol 2020; 63:9–14. [PubMed: 32062144]
5. Herzog W, and Weber K Fractionation of brain microtubule-associated proteins: isolation of two different proteins which stimulate tubulin polymerization in vitro. Eur. J. Biochem 1978; 92:1–8. [PubMed: 729584]
6. Lewis SA, Ivanov IE, Lee G-H, and Cowan NJ Organization of microtubules in dendrites and axons is determined by a short hydrophobic zipper in microtubule-associated proteins MAP2 and tau. Nature 1989; 342:498–505. [PubMed: 2511449]
7. Stearns ME, and Brown DL Purification of a microtubule-associated protein based on its preferential association with tubulin during microtubule initiation. FEBS Lett. 1979; 101:15–20. [PubMed: 446728]
8. Gamblin TC, Nachmanoff K, Halpain S, and Williams RC Recombinant microtubule-associated protein 2c reduces the dynamic instability of individual microtubules. Biochemistry 1996; 35:12576–12586. [PubMed: 8823195]
9. Doki C, Nishida K, Saito S, Shiga M, Ogara H, Kuramoto A, Kuragano M, Nozumi M, Igarashi M, Nakagawa H, Kotani S, and Tokuraku K Microtubule elongation along actin filaments induced by microtubule-associated protein 4 contributes to the formation of cellular protrusions. The Journal of Biochemistry 2020; 168:295–303. [PubMed: 32289170]
10. Dehmelt L, Smart FM, Ozer RS, and Halpain S The Role of Microtubule-Associated Protein 2c in the Reorganization of Microtubules and Lamellipodia during Neurite Initiation. J. Neurosci 2003; 23:9479–9490. [PubMed: 14573527]

11. Edson K, Weisshaar B, and Matus A Actin depolymerisation induces process formation on MAP2-transfected non-neuronal cells. Development 1993; 117:689–700. [PubMed: 8392463]
12. Bélanger D, Farah CA, Nguyen MD, Lauzon M, Cornibert S, and Leclerc N The projection domain of MAP2b regulates microtubule protrusion and process formation in Sf9 cells. J. Cell Sci 2002; 115:1523–1539. [PubMed: 11896199]
13. Leclerc N, Baas PW, Garner CC, and Kosik KS Juvenile and mature MAP2 isoforms induce distinct patterns of process outgrowth. Mol. Biol. Cell 1996; 7:443–455. [PubMed: 8868472]
14. Jalava NS, Lopez-Picon FR, Kukko-Lukjanov T-K, and Holopainen IE Changes in microtubule-associated protein-2 (MAP2) expression during development and after status epilepticus in the immature rat hippocampus. Int. J. Dev. Neurosci 2007; 25:121–131. [PubMed: 17229541]
15. Quinlan EM, and Halpain S Emergence of Activity-Dependent, Bidirectional Control of Microtubule-Associated Protein MAP2 Phosphorylation during Postnatal Development. J. Neurosci 1996; 16:7627–7637. [PubMed: 8922419]
16. Ozer RS, and Halpain S Phosphorylation-dependent Localization of Microtubule-associated Protein MAP2c to the Actin Cytoskeleton. Mol. Biol. Cell 2000; 11:3573–3587. [PubMed: 11029056]
17. Ferralli J, Doll T, and Matus A Sequence analysis of MAP2 function in living cells. J. Cell Sci 1994; 107:3115–3125. [PubMed: 7699010]
18. Eidenmüller J, Fath T, Maas T, Pool M, Sontag E, and Brandt R Phosphorylation-mimicking glutamate clusters in the proline-rich region are sufficient to simulate the functional deficiencies of hyperphosphorylated tau protein. Biochem. J 2001; 357:759–767. [PubMed: 11463346]
19. Biernat J, Gustke N, Drewes G, and Mandelkow E Phosphorylation of Ser262 strongly reduces binding of tau to microtubules: distinction between PHF-like immunoreactivity and microtubule binding. Neuron 1993; 11:153–163. [PubMed: 8393323]
20. Grubisha M, Sun X, MacDonald M, Garver M, Sun Z, Paris K, Patel D, DeGiosio R, Lewis D, and Yates N MAP2 is differentially phosphorylated in schizophrenia, altering its function. Mol. Psychiatry 2021; 26:5371–5388. [PubMed: 33526823]
21. Bonfils C, Bec N, Lacroix B, and Larroque C Kinetic analysis of tubulin assembly in the presence of the microtubule-associated protein TOGp. J. Biol. Chem 2007; 282:5570–5581. [PubMed: 17178729]
22. Doolittle LK, Rosen MK, and Padrick SB (2013) Measurement and analysis of in vitro actin polymerization. In Adhesion Protein Protocols pp. 273–293, Springer
23. Fujiwara I, Vavylonis D, and Pollard TD Polymerization kinetics of ADP-and ADP-Pi-actin determined by fluorescence microscopy. Proc. Nat. Acad. Sci 2007; 104:8827–8832. [PubMed: 17517656]
24. Murthy ASN, and Falvin M Microtubule assembly using the microtubule-associated protein MAP-2 prepared in defined states of phosphorylation with protein kinase and phosphatase. Eur. J. Biochem 1983; 137.
25. Itoh TJ, and Hotani H Microtubule-stabilizing activity of microtubule-associated proteins (MAPs) is due to increase in frequency of rescue in dynamic instability: shortening length decreases with binding of MAPs onto microtubules. Cell structure and function 1994; 19:279–290. [PubMed: 7850890]
26. BURNS RG, ISLAM K, and CHAPMAN R The multiple phosphorylation of the microtubule-associated protein MAP2 controls the MAP2: tubulin interaction. Eur. J. Biochem 1984; 141:609–615. [PubMed: 6146522]
27. Cooper JA, Walker SB, and Pollard TD Pyrene actin: documentation of the validity of a sensitive assay for actin polymerization. J. Muscle Res. Cell Motil 1983; 4:253–262. [PubMed: 6863518]
28. Bubb MR, Spector I, Beyer BB, and Fosen KM Effects of jasplakinolide on the kinetics of actin polymerization: an explanation for certain in vivo observations. J. Biol. Chem 2000; 275:5163–5170. [PubMed: 10671562]
29. Amniai L, Barbier P, Sillen A, Wieruszeski J-M, Peyrot V, Lippens G, and Landrieu I Alzheimer disease specific phosphoepitopes of Tau interfere with assembly of tubulin but not binding to microtubules. The FASEB Journal 2009; 23:1146–1152. [PubMed: 19074508]

30. Schwalbe M, Kadavath H, Biernat J, Ozenne V, Blackledge M, Mandelkow E, and Zweckstetter M Structural impact of tau phosphorylation at threonine 231. Structure 2015; 23:1448–1458. [PubMed: 26165593]

31. Savastano A, Jaipuria G, Andreas L, Mandelkow E, and Zweckstetter M Solid-state NMR investigation of the involvement of the P2 region in tau amyloid fibrils. Sci. Rep 2020; 10:1–14. [PubMed: 31913322]

32. Lu P-J, Wulf G, Zhou XZ, Davies P, and Lu KP The prolyl isomerase Pin1 restores the function of Alzheimer-associated phosphorylated tau protein. Nature 1999; 399:784–788. [PubMed: 10391244]

33. Koren J, Jinwal UK, Davey Z, Kiray J, Arulselvam K, and Dickey CA Bending tau into shape: the emerging role of peptidyl-prolyl isomerases in tauopathies. Mol. Neurobiol 2011; 44:65–70. [PubMed: 21523562]

34. Kapitein LC, Yau KW, Gouveia SM, van der Zwan WA, Wulf PS, Keijzer N, Demmers J, Jaworski J, Akhmanova A, and Hoogenraad CC NMDA receptor activation suppresses microtubule growth and spine entry. J. Neurosci 2011; 31:8194–8209. [PubMed: 21632941]

35. Roger B, Al-Bassam J, Dehmelt L, Milligan RA, and Halpain S MAP2c, but Not Tau, Binds and Bundles F-Actin via Its Microtubule Binding Domain. Curr. Biol 2004; 14:363–371. [PubMed: 15028210]

36. Elie A, Prezel E, Guérin C, Denarier E, Ramirez-Rios S, Serre L, Andrieux A, Fourest-Lieuvin A, Blanchoin L, and Arnal I Tau co-organizes dynamic microtubule and actin networks. Sci. Rep 2015; 5:9964. [PubMed: 25944224]

37. Kim Y, Jang Y-N, Kim J-Y, Kim N, Noh S, Kim H, Queenan BN, Bellmore R, Mun JY, Park H, Rah JC, Pak DTS, and Lee KJ Microtubule-associated protein 2 mediates induction of long-term potentiation in hippocampal neurons. The FASEB Journal 2020; 34:6965–6983. [PubMed: 32237183]

38. Mohan R, and John A Microtubule-associated proteins as direct crosslinkers of actin filaments and microtubules. IUBMB Life 2015; 67:395–403. [PubMed: 26104829]

39. Kim G, Choe Y, Park J, Cho S, and Kim K Activation of protein kinase A induces neuronal differentiation of HiB5 hippocampal progenitor cells. Mol. Brain Res 2002; 109:134–145. [PubMed: 12531523]

40. Vogt Weisenhorn DM, Roback LJ, Kwon JH, and Wainer BH Coupling of cAMP/PKA and MAPK Signaling in Neuronal Cells Is Dependent on Developmental Stage. Exp. Neurol 2001; 169:44–55. [PubMed: 11312557]

41. Shea TB, Beermann ML, Leli U, and Nixon RA Opposing influences of protein kinase activities on neurite outgrowth in human neuroblastoma cells: Initiation by kinase A and restriction by kinase C. J. Neurosci. Res 1992; 33:398–407. [PubMed: 1335089]

42. Mazel T, Biesemann A, Krejczy M, Nowald J, Müller O, and Dehmelt L Direct observation of microtubule pushing by cortical dynein in living cells. Mol. Biol. Cell 2014; 25:95–106. [PubMed: 24173713]

43. Bramblett GT, Goedert M, Jakes R, Merrick SE, Trojanowski JQ, and Lee VMY Abnormal tau phosphorylation at Ser396 in alzheimer's disease recapitulates development and contributes to reduced microtubule binding. Neuron 1993; 10:1089–1099. [PubMed: 8318230]

44. Regan P, Piers T, Yi J-H, Kim D-H, Huh S, Park SJ, Ryu JH, Whitcomb DJ, and Cho K Tau Phosphorylation at Serine 396 Residue Is Required for Hippocampal LTD. J. Neurosci 2015; 35:4804–4812. [PubMed: 25810511]

45. Cho J-H, and Johnson GVW Primed phosphorylation of tau at Thr231 by glycogen synthase kinase 3β (GSK3β) plays a critical role in regulating tau's ability to bind and stabilize microtubules. J. Neurochem 2004; 88:349–358. [PubMed: 14690523]

46. Cabrales Fontela Y, Kadavath H, Biernat J, Riedel D, Mandelkow E, and Zweckstetter M Multivalent cross-linking of actin filaments and microtubules through the microtubule-associated protein Tau. Nature Communications 2017; 8:1981.

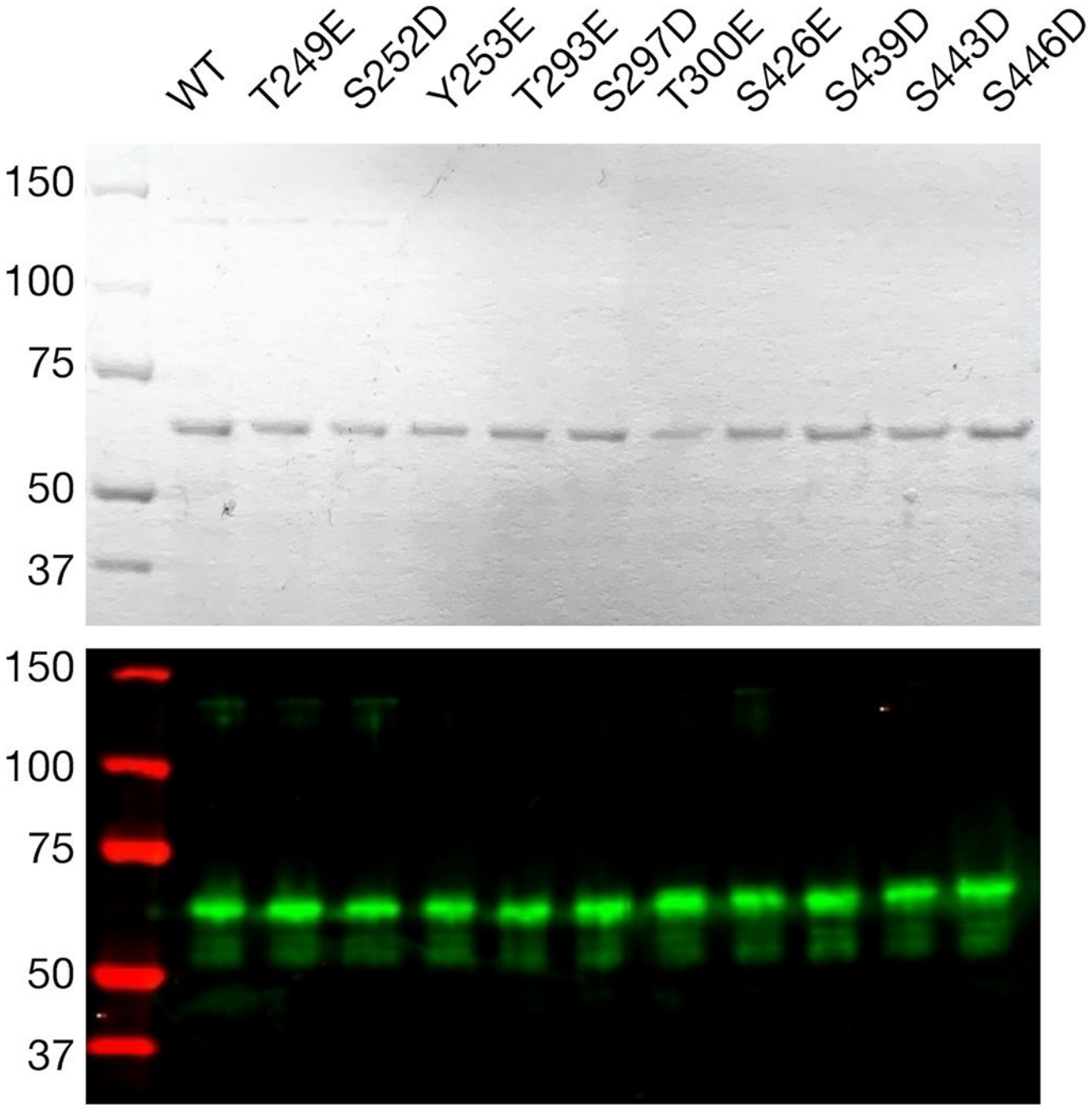

Figure 1. Isolated phosphomimetic MAP2C constructs.

Coomassie blue-stained SDS-PAGE gel (top) or western blot (bottom) of all MAP2C constructs used in the present study. Ladder band (far left) masses are in kDa. The predicted molecular weight of MAP2C is approximately 50 kDa but the protein typically migrates at ~70 kDa. Faint bands are observed at ~140 kDa and may reflect minor dimerization products.

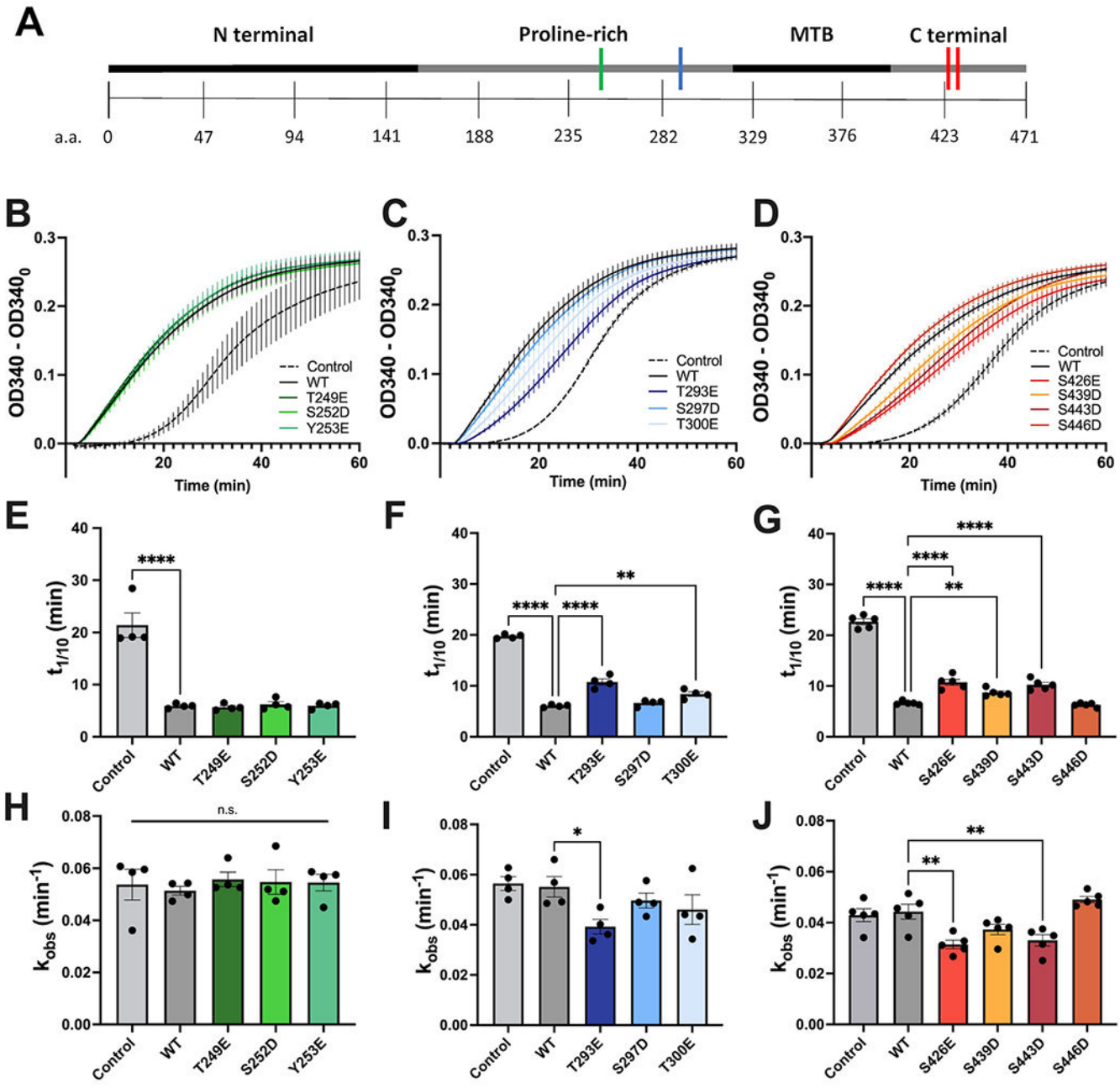

Figure 2. MAP2 phosphomimetic mutations in the C-terminal and proline-rich domain impair tubulin polymerization.

(A) Sequence map of the MAP2C protein. Positions of grouped phosphorylated sites are delineated with colored vertical lines. **(B-D)** Averaged polymerization curves for each group. Average is taken for each timepoint of the curve. All genotypes are compared to a reaction lacking MAP2 protein (Control). Vertical lines indicate SEM. **(E-G)** The presence of MAP2 significantly reduces tenth time ($t_{1/10}$), while several phosphomimetic mutants increase $t_{1/10}$ relative to WT. **(H-J)** The presence of MAP2 does not affect k_{obs}, the pseudo-first order rate constant of tubulin polymerization, yet several phosphomimetic constructs significantly reduce k_{obs} relative to WT. * $p < 0.05$; ** $p < 0.01$; **** $p < 0.0001$.

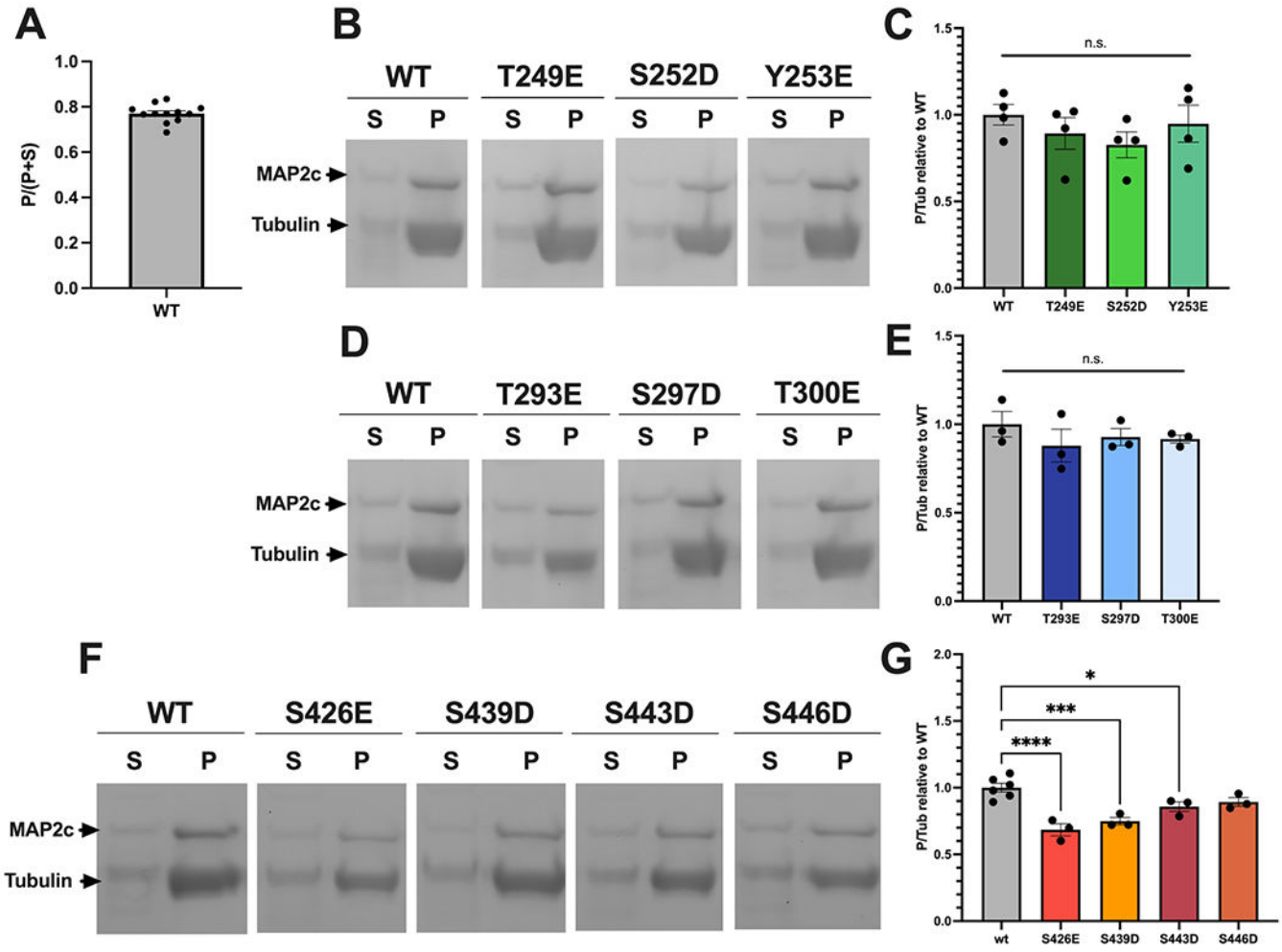

Figure 3. C-terminal MAP2 phosphomimetic mutations impair MT-binding.

(A) ~77% of WT MAP2 was pulled down in the ultracentrifugation-based assay. **(B,D,F)** Representative stained SDS polyacryamide gels are shown for each group. **(C,E,G)** Several C-terminal phosphomimetic constructs show reduced levels of pull-down with preassembled MTs relative to WT MAP2. S = supernatant, P = pellet, Tub = Tubulin band in P. * $p < 0.05$; *** $p < 0.001$; **** $p < 0.0001$.

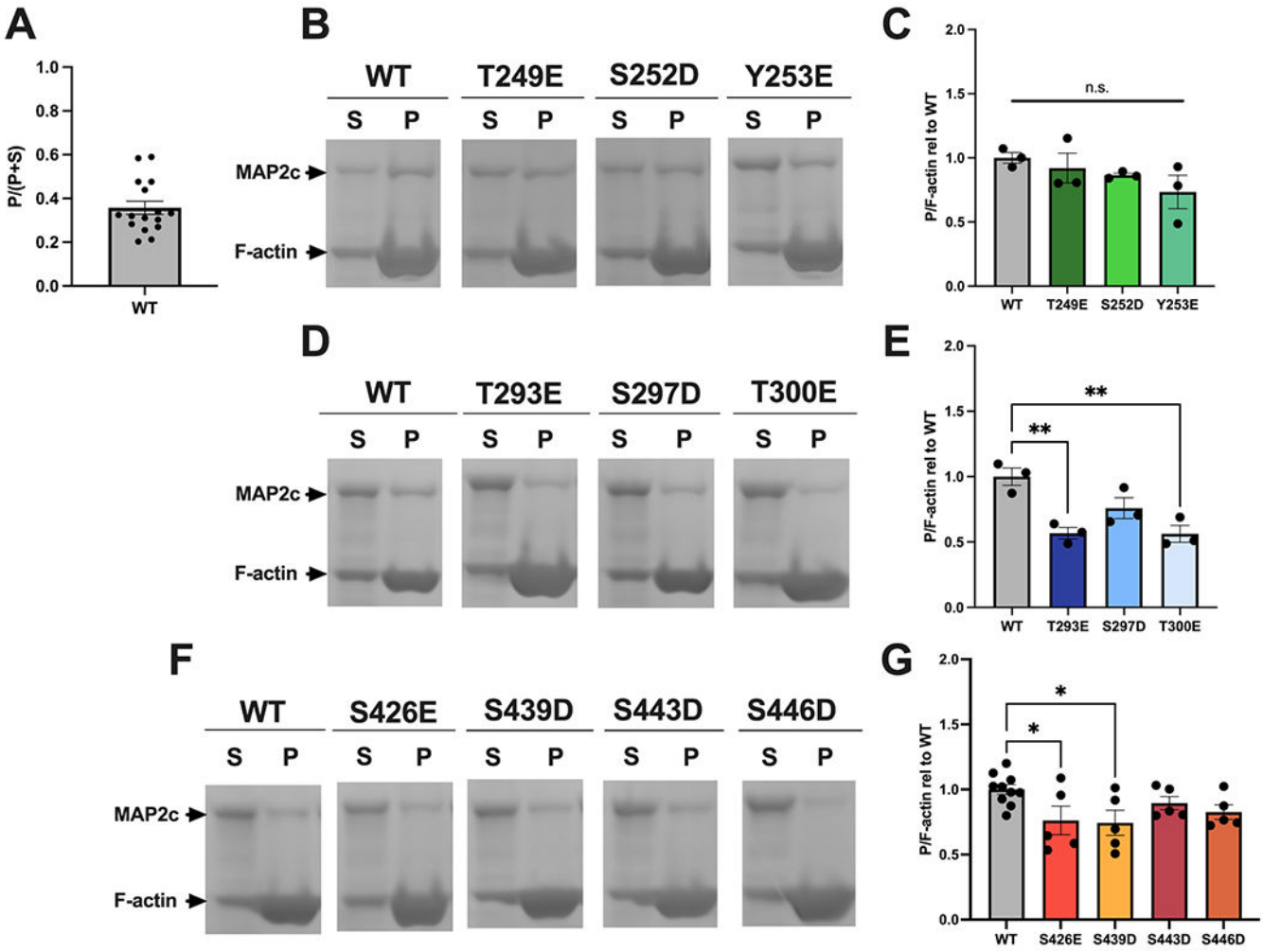

Figure 4. C-terminal and proline-rich domain MAP2 phosphomimetic mutations impair actin-binding.

(A) ~36% of WT MAP2 was pulled down in the ultracentrifugation-based assay. **(B,D,F)** Representative stained SDS polyacrylamide gels are shown for each group. **(C,E,G)** Several proline-rich and C-terminal phosphomimetic constructs show reduced pull-down with preassembled actin filaments relative to WT MAP2. S = supernatant, P = pellet, F-actin = actin band in P. * $p < 0.05$; ** $p < 0.01$.

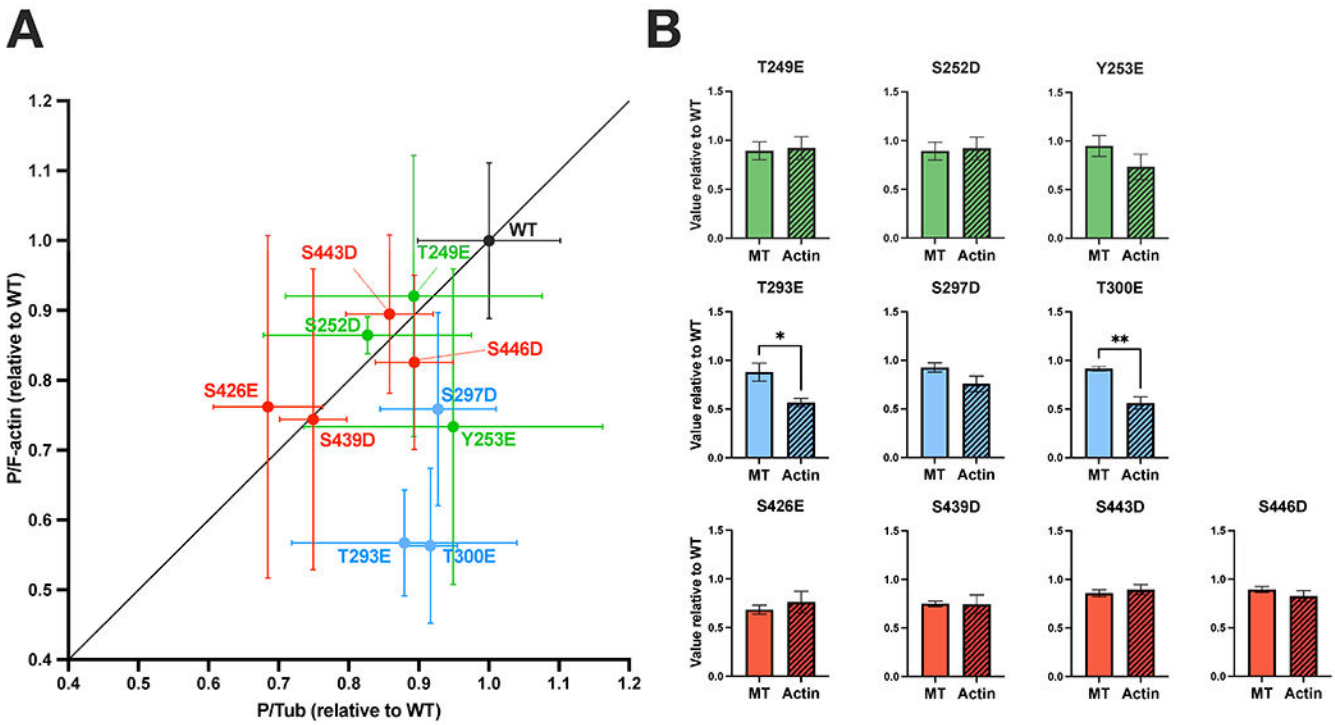

Figure 5. T293E and T300E have differential effects on MT- and actin-binding.

(A) An XY plot showing the relative MT-binding (X-axis) and actin-binding (Y-axis) (as defined by P/Tub and P/F-actin in Figures 3–4) of tested genotypes. The unity line (black line) represents equivalent changes in MT- and actin-binding capabilities relative to WT. Data are shown as mean ± standard deviation (SD). SD for WT was averaged across groups**.** **(B)** P/Tub (MT) and P/F-actin (Actin) values are compared within-genotype. * $p < 0.05$; ** $p < 0.01$.

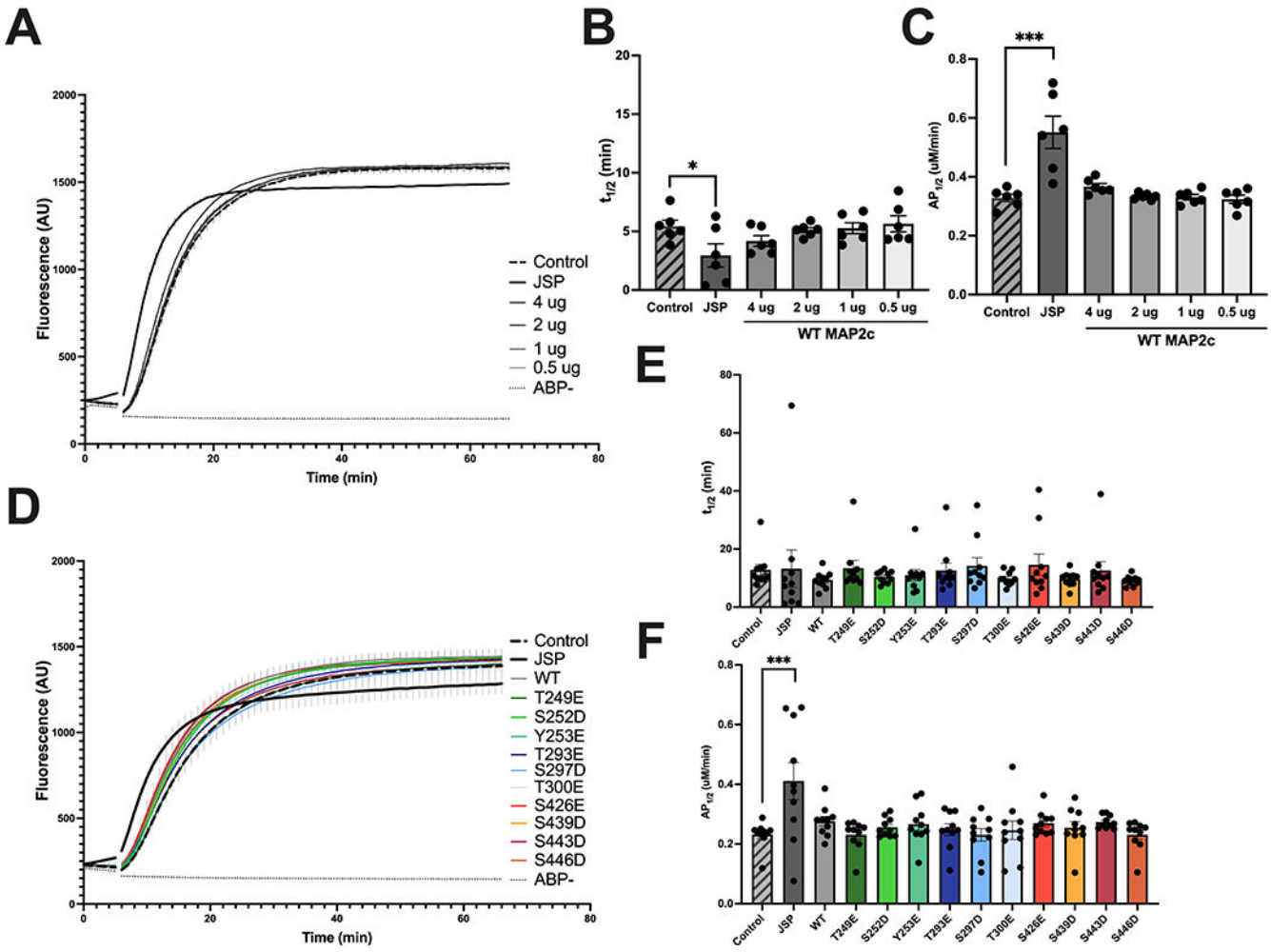

Figure 6. MAP2 does not regulate actin polymerization.

(A) Average polymerization curve for the indicated levels of MAP2. Data were also obtained for a positive control reaction containing jasplakinolide (JSP), a negative control reaction lacking MAP2 protein (Control), and a negative control reaction lacking actin polymerization buffer (ABP-) (see Materials & Methods). Average is taken for each timepoint of the curve. Vertical lines indicate SEM. **(B-C)** MAP2 fails to change the half-time of the reaction ($t_{1/2}$) **(B)** or the polymerization rate at $t_{1/2}$ ($AP_{1/2}$) **(C)**. **(D)** Average polymerization curve for all MAP2 genotypes (1 μg each) and JSP, Control and ABP- reactions. **(E-F)** All MAP2 genotypes fail to affect $t_{1/2}$ **(E)** or $AP_{1/2}$ **(F)**. * $p < 0.05$; *** $p < 0.001$.

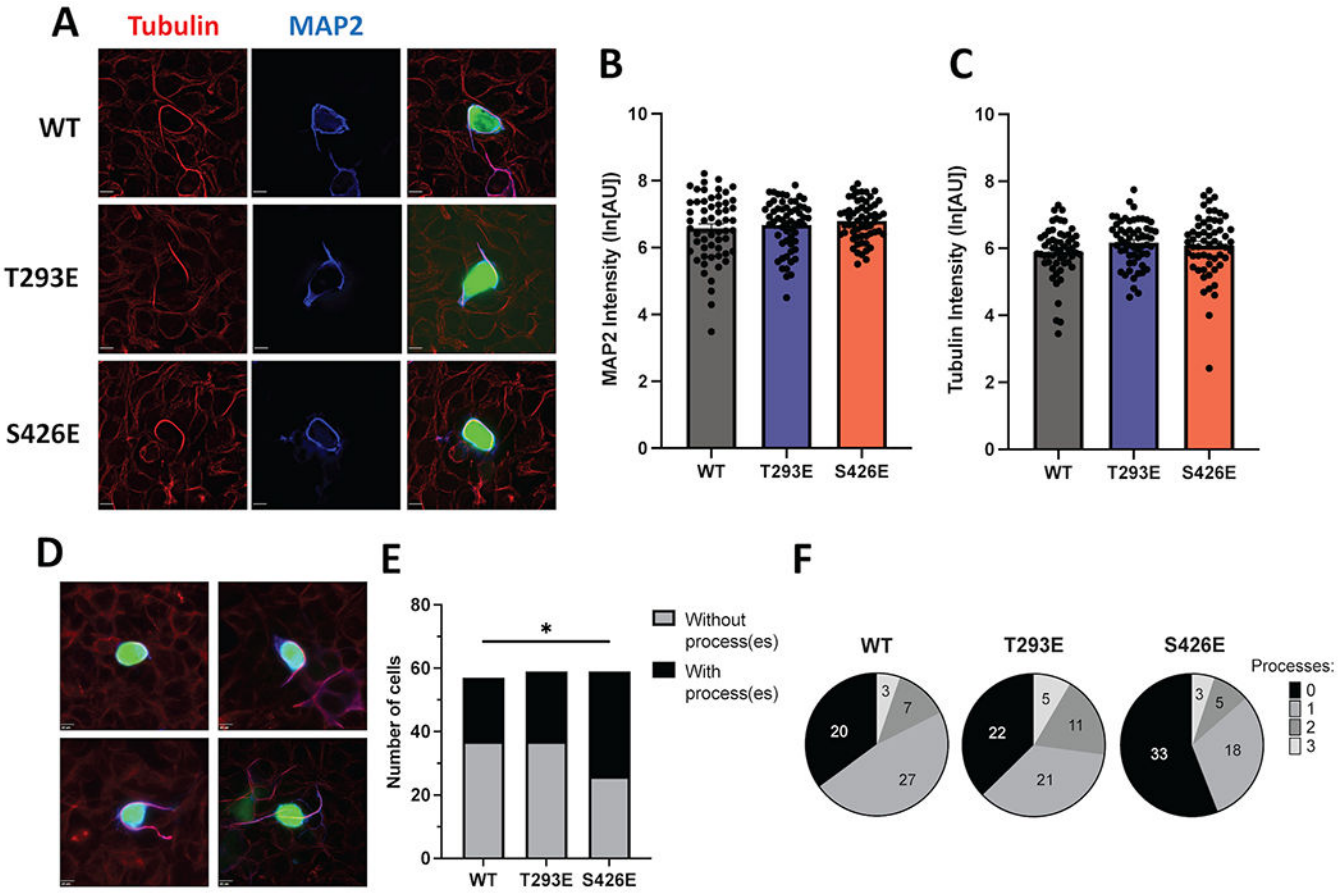

Figure 7. The S426E, but not the T293E, mutation impairs process formation in HEK293T cells.

(A) Exemplar images of transfected cells. Scale bars = 10 um. **(B-C)** Mean intensities of MAP2 **(B)** and β-tubulin **(C)**. **(D)** Exemplar images of cells with 0 (top left), 1 (top right), 2 (bottom left) or 3 (bottom right) process(es). Scale bars = 10 um. **(E)** Number of cells with or without at least 1 process per genotype. **(F)** Frequencies for number of processes per genotype. Numbers within the pie charts represent cells counted per category.

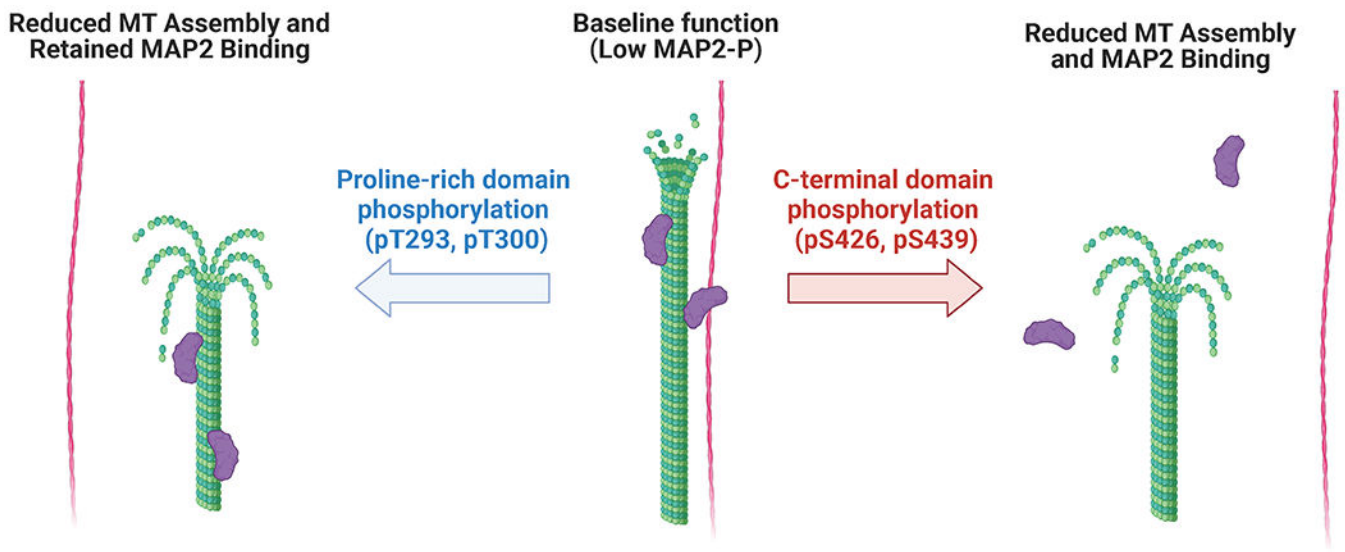

Figure 8. Model of MAP2 regulation by phosphorylation in proline-rich and C-terminal domains.

Diagram of functional consequences resulting from MAP2-P. When MAP2 is relatively dephosphorylated (middle), MAP2 (purple) binds and crosslinks MTs (green) and actin (red) while promoting MT assembly. We here represent this crosslinking function as a multivalent interaction with both filaments by a single MAP2 molecule, as has been suggested for Tau[46]. Following phosphorylation of MAP2 at sites in the proline-rich domain (left), the ability of MAP2 to assemble MTs is reduced (either due to increased incidence of catastrophe [pictured], or reduced rates of polymerization and/or bundling). MT/actin crosslinking is also presumed to be disrupted, as actin-binding affinity is reduced. However, MT-binding is preserved. After MAP2-P in C-terminal domain sites (right), MAP2 partially dissociates from both MTs and actin, also concurrent with reduced MT assembly and a presumed reduction in MT/actin crosslinking. Created with BioRender.com.

Table 1.
Primers used for cloning and mutagenesis.

Targeted codon is denoted in bold face.

TARGET	FORWARD (5′-3′)	REVERSE (5′-3′)
NdeI-MAP2c-XhoI	taaacgcatatggcagatgaacggaaagatgaag	tcagtcatcggtctcgagctacaagccctgc
MAP2c T249E	ctactgccatcactcctggc**gaa**ccaccaagttattcttcacg	cgtgaagaataacttggtgg**ttc**gccaggagtgatggcagtag
MAP2c S252D	catcactcctggcaccccacca**gat**tattcttcacgcacacc	ggtgtgcgtgaagaata**atc**tggtggggtgccaggagtgatg
MAP2c Y253E	catcactcctggcaccccaccaagt**gaa**tcttcacgcacac	gtgtgcgtgaaga**ttc**acttggtggggtgccaggagtga
MAP2c T293E	tgagaagaaggtcgccatcatacgt**gaa**cctccaaaatctcctgc	gcaggagattttggagg**ttc**acgtatgatggcgaccttcttctca
MAP2c S297D	cgccatcatacgtactcctccaaaa**gat**cctgcgactccc	gggagtcgcagg**atc**ttttggaggagtacgtatgatggcg
MAP2c T300E	cctccaaaatctcctgcg**gaa**cccaagcagcttcggctt	aagccgaagctgcttggg**ttc**cgcaggagattttggagg
MAP2c S426E	ggctgagatcattacacag**gaa**ccaggcagatccagcgtgg	ccacgctggatctgcctgg**ttc**ctgtgtaatgatctcagcc
MAP2c S439D	catcaccccgacgactc**gac**aatgtctcctcgtctg	cagacgaggagacatt**gtc**gagtcgtcggggtgatg
MAP2c S443D	gacgactcagcaatgtctccgattctg**gaa**gcatcaacctgct	agcaggttgatgc**ttc**cagaatcggagacattgctgagtcgtc
MAP2c S446D	caatgtctcctcgtctgga**gac**atcaacctgctcgaatct	agattcgagcaggttgat**gtc**tccagacgaggagacattg